Atmos. Chem. Phys. Discuss., doi:10.5194/acp-2016-494, 2016
Manuscript under review for journal Atmos. Chem. Phys.
Published: 23 June 2016

Atmospheric Chemistry and Physics Discussions

Direct observations of organic aerosols in common wintertime hazes in North China: insights into their size, shape, mixing state, and source

S. R. Chen[1], L. Xu[1], Y. X. Zhang[1], B. Chen[1], X. F. Wang[1], X. Y. Zhang[2], M. Zheng[3], J. M. Chen[1], W. X. Wang[1], Y. L. Sun[4], P. Q. Fu[4], Z. F. Wang[4], W. J. Li[1,*]

[1] Environment Research Institute, Shandong University, Jinan, Shandong 250100, China

[2] Key Laboratory of Atmospheric Chemistry, Chinese Academy of Meteorological Sciences, Beijing 100081, China

[3] State Key Joint Laboratory of Environmental Simulation and Pollution Control, College of Environmental Sciences and Engineering, Peking University, Beijing 100871, China

[4] State Key Laboratory of Atmospheric Boundary Layer Physics and Atmospheric Chemistry, Institute of Atmospheric Physics, Chinese Academy of Sciences, Beijing, China

[*]Corresponding Email: liweijun@sdu.edu.cn (W. J. Li)

Atmos. Chem. Phys. Discuss., doi:10.5194/acp-2016-494, 2016
Manuscript under review for journal Atmos. Chem. Phys.
Published: 23 June 2016

Abstract

Many studies have focused on the physicochemical properties of aerosol particles in unusually severe haze episodes instead of the more freqent and less severe hazes. Consistent with this lack of attention, the morphology and mixing state of organic matter (OM) particles in the frequent light and moderate (L&M) hazes in winter in North China Plain (NCP) have not been examined, even though OM dominates these fine particles. In the present work, morphology, mixing state, and size of organic aerosols in the L&M hazes were systematically characterized using transmission electron microscopy coupled with energy-dispersive X-ray spectroscopy, atomic force microscopy, and nanoscale secondary ion mass spectrometer, with the comparisons among an urban site (Jinan, S1), a mountain site (Tai, S2), and a background island site (Changdao, S3) in the same hazes. Based on their morphology, the OM particles were divided into six different types: spherical (type 1), near-spherical (type 2), irregular (type 3), domelike (type 4), dispersed-OM (type 5), and OM-coating (type 6). In the three sampling sites, type 1-3 of OM particles were most abundant in the L&M hazes and most of them were internally mixed with non-OM particles. The abundant near-spherical OM particles with higher sphericity and lower aspect ratio indicate that these primary OM particles formed in cooling, polluted plumes from coal combustion and biomass burning. Based on the Si-O-C ratio in OM particles, we estimated that 71% of type 1-3 OM particles were associated with coal combustion. Our result suggests that coal combustion in residential stoves was a widespread source from urban to rural areas in the NCP. Average OM thickness which correlates with the age of the air masses in type 6 particles only slightly increased from S3 to S2 to S1, suggesting that the L&M hazes were usually dry (relative humidity < 60%) with weak photochemistry and heterogeneous reactions between aerosols and gases. We conclude that the direct emissions from these coal stoves without any pollution controls in rural areas and in urban outskirts mainly contribute into the regional L&M hazes in North China.

Atmos. Chem. Phys. Discuss., doi:10.5194/acp-2016-494, 2016
Manuscript under review for journal Atmos. Chem. Phys.
Published: 23 June 2016

1 Introduction

Atmospheric particulate matter is composed of diverse chemical compounds, both organic and inorganic matters. Organic aerosol particles are of two types: primary organic aerosol (POA), directly emitted from fossil fuel combustion, biomass burning, vehicular exhaust, and cooking; and secondary organic aerosol (SOA), formed from the oxidation of gaseous volatile organic compounds (Kanakidou et al., 2005). Organic aerosols account for 18-70% of the non-refractory submicron aerosol particles in the atmosphere (Zhang et al., 2007). It is well known that organic aerosols affect the atmosphere through the interaction with reactive trace gases, water vapor, clouds, precipitation, and radiation (Fuzzi et al., 2006). Organic aerosols also influence the physical and chemical properties of atmospheric particles (e.g., size, light-absorptivity, and hygroscopicity); they directly affect visibility and climate by scattering and absorbing solar radiation (Poschl, 2005;Kanakidou et al., 2005;Kulmala et al., 2004). Although most organic aerosol components are known to have a cooling effect on global climate, brown carbon in organic aerosols can absorb solar radiation at shorter wavelengths and lead to warming (Alexander et al., 2008). Moreover, many organic compounds (e.g., benzene, polycyclic aromatic hydrocarbons (PAHs), toluene), which are toxic to human and other biological species have been found in atmospheric particles (Mauderly and Chow, 2008).

In recent years, haze episodes have become one of the most serious environment problems in China, following the rapid urbanization and population growth in eastern China. China's Ministry of Environmental Protection on 1 January 2013, started to monitor daily $PM_{2.5}$ concentrations and defined the various air pollution levels as: excellent (0~35 μg m^{-3}), good (35~75 μg m^{-3}), light (75~115 μg m^{-3}), moderate (115~150 μg m^{-3}), heavy (150~250 μg m^{-3}), and severe (> 250 μg m^{-3}) (HJ 663-2012). Haze as a weather phenomenon is defined by visibility ≤ 10 km and RH ≤ 95%. Previous studies have shown that haze levels normally are associated with $PM_{2.5}$ concentrations and RH (Shen et al., 2015;Wang et al., 2006;Chen et al., 2014). Based on their results, we classify severe haze days (< 5 km) with $PM_{2.5}$ concentrations ≥

Atmos. Chem. Phys. Discuss., doi:10.5194/acp-2016-494, 2016
Manuscript under review for journal Atmos. Chem. Phys.
Published: 23 June 2016

250 μg m^{-3} and light (8-10 km) to moderate (5-8 km) haze days at 75-250 μg m^{-3}, both with RH < 80%.

Severe wintertime haze pollution episodes were driven to a large extent by secondary aerosol formation, and SOA were found to be of similar importance with secondary inorganic aerosols (Guo et al., 2014;Huang et al., 2014). However, Sun et al. (2013) showed that OM was dominant in wintertime haze pollution episodes but POA concentrations were much higher than SOA in the aerosol particles. The reason about the different results of OM particles among these studies could be the difference of air pollution levels and RH during the haze pollution episodes. Severe winter hazes were driven by stable synoptic meteorological conditions with high relative humidity (i.e., RH > 80% frequently or consistently occurred during the haze episodes) (Tie et al., 2015). Due to the dimming effect of high-concentration aerosol particles, an enhanced production rate of secondary aerosols was suggested as an important contribution from the complicated heterogeneous reactions (Li et al., 2011c;Zheng et al., 2015). Because of severe haze episodes with unusually high $PM_{2.5}$ concentrations (> 250 μg m^{-3}) and low visibility (< 5 km), many scientists have been investigated the physicochemical properties of their aerosol particles (Huang et al., 2014;Guo et al., 2014;Zheng et al., 2015). Although this knowledge is critical to understand severe haze formation and its impacts on human health, the frequency of severe haze events is low, they are of short duration. For example, we statistically analyzed haze days during the winter (~ 92 days) of 2014-2015 in nine different cities. Figure S1 shows that light and moderate (L&M) haze days occurred 22-63% of the time and that severe haze days were less frequent at 4-32%, with the variation dependent on location within the NCP. As we know, the L&M hazes are precursors of severe ones. Zheng et al. (2015) suggested that characteristics of aerosol particles in severe hazes would not be the same in L&M hazes. Compared to severe hazes, the L&M hazes were most frequent in winter and lasted longer in the NCP. Therefore, understanding aerosol particles in the more common L&M hazes in the NCP is important to further evaluate their impacts on human health and regional climate.

Atmos. Chem. Phys. Discuss., doi:10.5194/acp-2016-494, 2016
Manuscript under review for journal Atmos. Chem. Phys.
Published: 23 June 2016

Various ''bulk'' analytical instruments have been used to study organic aerosol particles during haze episodes. High resolution time-of-flight aerosol mass spectrometry (HR-AMS) was applied to determine the mass concentrations and bulk composition of organic aerosols (Sun et al., 2010). Gas chromatography-mass spectrometry (GC-MS) provided chemical composition and structures of organics in aerosols (Fu et al., 2012;Wang et al., 2009). It should be noted that bulk analytical techniques only provide average properties of $PM_{2.5}$ and the mixing state, phase, and morphology of organic particles remain unknown. Detailed information about individual organic particles, moreover, is critical to evaluate their formation, their sources, and their hygroscopic and optical properties in the atmosphere. For example, copious tar balls containing homogeneous BrC ocurr in the smoldering smoke from biofuels (Chakrabarty et al., 2010;Adachi and Buseck, 2011;Alexander et al., 2008;Chakrabarty et al., 2013;China et al., 2013;Hand et al., 2005;Posfai et al., 2004). Atmospheric particles undergo liquid-liquid phase separations and go on to form OM coatings on inorganic aerosol particles (You et al., 2012). The surface coating by OM on individual particles influences water uptake and evaporation of inidividual particles and their heterogeneous reactions in the atmosphere (Shiraiwa et al., 2011;Zawadowicz et al., 2015;Riipinen et al., 2011). Despite the importance of these phenomena, the morphology and mixing state of OM particles in wintertime L&M hazes in the NCP have not been examined, although OM is dominant in fine particles (Sun et al., 2013).

To characterize organic aerosols in greater detail in L&M hazes, individual particles in the NCP in winter were analyzed using transmission electron microscopy coupled with energy-dispersive X-ray spectroscopy (TEM/EDX), atomic force microscopy (AFM), and Nanoscale secondary ion mass spectrometer (NanoSIMS). Aerosol particles were simultaneously collected on TEM grids in the NCP during 13-23 December, 2014. Morphology, mixing state, and size of organic aerosols were systematically characterized and compared at the three sampling sites (background island site, mountain site, and urban site) in the same haze. This information enables

Atmos. Chem. Phys. Discuss., doi:10.5194/acp-2016-494, 2016
Manuscript under review for journal Atmos. Chem. Phys.
Published: 23 June 2016

the discussion of source and ageing mechanisms of OM particles, which leads to insights about the formation of regional wintertime L&M hazes in the NCP.

2 Experimental Methods

2.1 Sampling sites and particle collection

$PM_{2.5}$ and individual particle samples were simultaneously collected during 13-23 December, 2014 at three sampling sites: an urban site (S1), a mountain site (S2), and a background site (S3) in the NCP (Fig. 1). S1- the urban site in Jinan (36.67 °N, 116.98 °E) is 50 km north of S2. S1 is a typical polluted city with high-density residential areas surrounded by large industrial zones (Li et al., 2011c). Aerosol particles collected at S1 mainly reflect local, ground-based urban and industrial emissions. S2-Mt. Tai (1534 m a.s.l., 36.251 °N, 117.101 °E) is the highest mountain in the middle of the NCP, ~230 km inland from the Bohai and Yellow Seas. S2 is the perfect location to observe air pollutants near the planetary atmospheric layer over the NCP. Aerosol particles collected at S2 represent regional transport (Li et al., 2011a). S3-Changdao Island, the National Station for Background Atmospheric Monitoring site (38.19 °N, 120.74 °E), is in the Bohai Sea. During the winter monsoon season, S3 is the downwind of the Jing-jin-ji area (i.e., Beijing city, Tianjin city, and Hebei province) and Shandong province. Therefore, S3 serves as a polluted background site from the transport of continental air. Therefore, aerosol particles collected at the three sampling sites display the different pollutant characteristics of polluted urban air, upper air layer, and background island air in the NCP.

$PM_{2.5}$ was collected on 90 mm quartz filters for 9-11.5 h using three KB-120 samplers at a flow rate of 100 L/min. The quartz filters were stored in a refrigerator for OC, EC, and water soluble ion analysis. In the study, OC and EC concentrations of 70 quartz filters were analyzed by an OC/EC analyzer (Sunset Lab) and water-soluble ions (i.e., K^+, Na^+, Ca^{2+}, Mg^{2+}, NH_4^+, F^-, SO_4^{2-},NO_3^-, and Cl^-) by an ion chromatography system (Dionex ICs-90). Three single-stage cascade impactors with a 0.5-mm diameter jet nozzle at a flow rate of 1.0 L/min were used to collect aerosols

Atmos. Chem. Phys. Discuss., doi:10.5194/acp-2016-494, 2016
Manuscript under review for journal Atmos. Chem. Phys.
Published: 23 June 2016

Atmospheric Chemistry and Physics Discussions

onto copper TEM grids coated with carbon film (carbon type-B, 300-mesh copper, Tianld Co., China). The collection efficiency of the impactor is 50% for particles with an aerodynamic diameter of 0.25 μm and with a density of 2 g cm^{-3} (Li et al., 2011a). After sample collection, the Cu grids were placed in a sealed, dry and clean environment until the TEM analysis. 11 aerosol samples at each sampling site were selected and analyzed by the TEM.

2.2 TEM analyses

The JEOL JEM-2100 transmission electron microscopy operated at 200 kV with energy-dispersive X-ray spectrometry (TEM/EDX) was used to analyze individual particles. An energy-dispersive X-ray spectrometer (EDX) can detect elements heavier than carbon. EDX spectra were executed for 15 s to minimize the potential beam damage. TEM grids are made of copper (Cu), so the Cu element will be excluded in the analyses. The distribution of particles on the TEM grids was not uniform: coarser particles were deposited near the center and finer particles dispersed on the fringe. To make sure that the analyzed particles were representative of the entire size range, three to four areas were chosen from the center and periphery of the sampling spot on each sample.

2.3 NanoSIMS analysis

Individual aerosol particles were analyzed using a nanoscale secondary ion mass spectrometer (NanoSIMS) 50L, an ultrahigh vacuum technique for surface and thin-film analysis at the Institute of Geology and Geophysics, Chinese Academy of Sciences. In this study, $^{12}C^-$, $^{16}O^-$, $^{12}C^{14}N^-$, $^{14}N^{16}O_2^-$, $^{32}S^-$ ions in individual particles were obtained when the Cs+ primary ion beam caused the ionization of atoms within the particles. Furthermore, ion intensity mappings of individual particles with nanometer resolution can show the distribution of different ions. $^{12}C^-$ and $^{12}C^{14}N^-$ represent the organic matter in individual particles (Chi et al., 2015;Ghosal et al., 2014;Li et al., 2016a).

2.4 AFM analysis

Atmos. Chem. Phys. Discuss., doi:10.5194/acp-2016-494, 2016
Manuscript under review for journal Atmos. Chem. Phys.
Published: 23 June 2016

Atmospheric Chemistry and Physics Discussions

Atomic force microscopy (AFM) with a tapping mode analyzed aerosol particles under ambient conditions. AFM, a digital NanoscopeIIIa Instrument, can determine the three dimensional morphology of particles. The AFM settings contain imaging forces between 1 and 1.5 nN, scanning rates between 0.5 and 0.8 Hz, and scanning range sizes at 10 μm with a resolution of 512 pixels per length. After the AFM analysis, composition of the same particles was confirmed by TEM, with 20, 25, and 13 individual particles analyzed by this method for each of the three sampling sites. The Nanoscope analysis software can automatically obtain bearing area (A) and bearing volume (V) of each analyzed particle according to the formulas described by Chi (Chi et al., 2015).

The relationship is shown in Figure S2 (EVD=0.8334ECD (S1), EVD=0.7286ECD (S2), and EVD=0.6601ECD (S3)). Therefore, the equivalent circle diameter (ECD, x) of individual aerosol particles measured from the iTEM software can be further converted into equivalent volume diameter (EVD, y) based on these relationships.

3. Results

3.1 Regional haze periods in North China Plain

Aerosol particles were collected in three regional L&M hazes during 13-23 December, 2014 (Fig. S3). Moderate Resolution Imaging Spectroradiometer (MODIS) images clearly display a regional haze layer covering the three sampling sites in the NCP (Fig. 1). The average $PM_{2.5}$ concentrations were 96.6 μg m^{-3} (range: 79-171 μg m^{-3}), 88.6 μg m^{-3} (range: 76-110 μg m^{-3}), and 80.3 μg m^{-3} (range: 75-84 μg m^{-3}) on haze days, twice as high as on clear days (52, 48, and 32.3 μg m^{-3}) at S1, S2, and S3, respectively. The RH at all three sampling sites was lower than 60% during the sampling periods (Fig. S4).

Figure 1 shows similar back trajectories of air masses at S1, S2, and S3. Haze episodes started to form in the NCP when air masses changed from north to southwest or west. Therefore, the regional hazes in the NCP were controlled by the same

Atmos. Chem. Phys. Discuss., doi:10.5194/acp-2016-494, 2016
Manuscript under review for journal Atmos. Chem. Phys.
Published: 23 June 2016

meteorological conditions (e.g., RH, temperature, and wind). The average concentrations of OC, EC, OC/EC, water-soluble ions and their mass proportions in $PM_{2.5}$ were much higher on haze days than on clear days at the three sampling sites (Table S1). OC on haze days was more than 1.7 times higher than that on clear days at three sites. OM concentration was estimated at 20-33 μg m^{-3} and $OM/PM_{2.5}$ ratio was at the range of 23-34% during haze days in the NCP (Table S1).

3.2 Morphology of organic particles

TEM/EDX identified five types of particles during the haze episodes: sulfates (including K-rich sulfate and ammonium sulfate), fly ash, mineral, soot, and C-dominated particles (Fig. S5). These results are consistent with previous studies during the haze episodes in the NCP (Li et al., 2012;Li et al., 2011c). In order to remove the interference of the carbon substrate on TEM grids, a nanoSIMS was employed to verify C-dominated particles through $^{12}C^{14}N^-$ and $^{12}C^-$ mappings (Fig. 2 and Fig. S6). Figure 2 clearly shows that one near-spherical particle, which contains C, O, and minor Si on TEM grids, displays strong CN^- and O^- signals but no clear NO_2^- and S^- signals. As a result, this type particle can be confirmed as the OM particle (Li et al., 2016a;Ghosal et al., 2014). TEM analysis showed that OM-containing particles were most abundant in all the haze samples, accounting for 70% of the 5090 analyzed particles (Fig. S7).

Based on the morphology of OM particles, they were divided into six different types: spherical (type 1, Fig. 3a), near-spherical (type 2, Fig. 3b)), irregular (type 3, Fig. 3c), domelike (type 4, Fig. 3d), dispersed-OM (type 5, Fig. 3e), and OM-coating (type 6, Fig. 3f). Because the high-resolution TEM images of individual particles can clearly display particle interior mixing structures, it allows us to identify OM particles based on their different shapes in OM-containing particles (Fig. S5). Figure 4 shows that the proportions of type 1-3 in OM particles was 73%, following type 4 at 5%, type 5 at 13%, and type 6 at 14%. Further, we measured the projected area, the perimeter, the maximum projected length, and the maximum projected width of 967 selected OM particles. From these data, the sphericity (Sph) and aspect ratio (AR) of

Atmos. Chem. Phys. Discuss., doi:10.5194/acp-2016-494, 2016
Manuscript under review for journal Atmos. Chem. Phys.
Published: 23 June 2016

different types of OM particles were calculated, which characterize their shape and thereby imply their aging during transport and their emission sources (Li et al., 2016b). The Sph and AR were defined by the following formulas referred to by (Li et al., 2013).

Aspect Ratio (AR). The maximum ratio of width and height of a bounding rectangle for the measured object is the aspect ratio. An aspect ratio of 1 (the lowest value) indicates a particle is not elongated in any direction.

Sphericity (Sph). Sphericity describes the sphericity or "roundness" of the measured object by using central moments. A sphericity of 1 (the highest value) indicates a particle is perfectly spherical.

$$Sph = \frac{\sqrt{4\pi S}}{P} = \frac{\sqrt{4\pi\pi R_1^2}}{2\pi R_2} = \frac{R_1}{R_2} \quad (1)$$

$$AR = \frac{L_{max}}{W_{max}} \quad (2)$$

Where S is projected area, R_1 is equivalent area radius, P is perimeter, R_2 is equivalent perimeter radius, L_{max} is the maximum projected length, and W_{max} is the maximum projected width.

Table 1 displays the Sph and AR of individual OM particles measured by the iTEM software. At the three different sampling sites, OM particles were in the fine range with diameters < 1 μm. The statistics show that spherical OM particles exhibited the highest Sph at 0.96-0.99 and the lowest AR at 1.0-1.03 at the three sites, followed by OM coating (Sph: 0.88-0.93, AR: 1.06-1.08), near-spherical OM (Sph: 0.82-0.83, AR: 1.12-1.13), domelike OM (Sph: 0.64-0.73, AR: 1.24-1.35), irregular OM (Sph: 0.50-0.57, AR: 1.39-1.48) and dispersed-OM particles (Sph 0.49-0.58, AR: 1.35-1.46).

3.3 Mixing state of OM particles

Although we identified different types of OM particles in individual particles, 86% were internally mixed with non-OM particles, such as soot, mineral, metal, fly ash, and sulfate particles (Fig. S5). Based on their morphological mixing state, we

Atmos. Chem. Phys. Discuss., doi:10.5194/acp-2016-494, 2016
Manuscript under review for journal Atmos. Chem. Phys.
Published: 23 June 2016

discriminated four OM internally mixed particles: OM-soot (Fig. 5a and Fig. S8), OM-mineral/metal (Fig. 5b), OM-fly ash (Fig. 5c), and OM-sulfate particles (Fig. 5d-e). Our results show that 83% of type 1-4 OM particles were attached to soot, mineral, sulfate, and metal particles, only 17% of type 1-4 OM particles were externally mixed particles, and all the type 5-6 OM were internally mixed with sulfate particles (Fig. S7).

Figure 6 shows number fractions of OM internally mixed particles in different size bins from 0.04 to 4.5 μm at the three sampling sites. OM-soot particles commonly occurred at S1 but they were mixed with certain amounts of sulfates at S2 and S3 during the sampling period (Fig. S8). The major OM internally mixed particles include 45% OM-soot particles and 46% OM-sulfate particles at S1, 35% and 62% at S2, 33% and 56% at S3 (Fig. S7). As a result, the number fraction of OM-sulfate particles increases from S1 to S2 and S3. OM-soot containing particles dominated in the finer size range (< 300 nm) at the three sampling sites (Fig. 6). In addition, 19% of OM-sulfate particles were internally mixed with inclusions (i.e., fly ash and metal) at all the three sampling sites (Fig. S7).

3.4 Size distribution of OM-containing particles

Figure 7 shows size distributions of OM-containing particles at the three sampling sites. Aerosol particles collected at S2 and S3 display a similar peak at ~400 nm, much smaller than the peak at 600 nm at the S1 site (Fig. 7a). This result indicates that sizes of locally emitted OM-containing particles are much larger than the long-range transported OM-containing particles. We further obtain size distributions of type 1-3 OM particles at the three sampling sites during one haze episode. Interestingly, type 1-3 OM particles displayed similar peaks around 350 nm at all three sampling sites (Fig. 7b). This result suggests that the OM sources were similar under different transport ranges in the same haze layer over the NCP.

4. Discussion

4.1 Sources of OM-containing particles

Atmos. Chem. Phys. Discuss., doi:10.5194/acp-2016-494, 2016
Manuscript under review for journal Atmos. Chem. Phys.
Published: 23 June 2016

TEM adequately characterized the morphology and mixing state of OM-containing particles in wintertime L&M hazes. We found that the type 1-3 OM particles (Fig. 3a-c) were most abundant in the hazes and that most of them were internally mixed with non-OM particles. This result is consistent with one previous study which found abundant amorphous spherical OM particles in the outflow of a haze plume in East Asia (Zhu et al., 2013). Moreover, Li et al. (2012) found large amounts of type 1 OM particles in a coal-burning region in the China Loess Plateau in winter. However, some studies found abundant type 5-6 OM particles in the atmosphere. For example, Moffet et al. (2013) suggested that OM coating particles become dominant following particle transport from an urban to background site and they didn't report abundant type 1-3 OM particles in North America. Also, Adachi et al. (2014) only reported that most sulfate particles were coated by secondary OM coating in remote mountain air in Japan. Based on these comparisons, we conclude that those type 1-3 OM particles were not emitted by vehicular emissions in the NCP.

It should be noted that recent studies did not find abundant type 1-3 OM particles at three sampling sites on haze episodes in spring and summer (Li et al., 2011b;Yuan et al., 2015). Zhang et al. (2008) suggested that industrial boilers had cleaner combustion with much less by-product of particulate carbon and with much lower levels of OM, while residential stoves had significantly higher emissions of carbonaceous particulate matter with emission rates 100 times higher than that of industrial boilers. As a result, we believe that the type 1-3 OM particles were not emitted from heavy industries or coal-fired power plants but, instead, they were from coal combustion or biomass burning for household heating and cooking in wintertime. In particular, the abundant near-spherical OM particles with higher Sph and lower AR indicate that these OM particles formed in cooling, polluted plumes from coal combustion and biomass burning.

Biomass burning and coal combustion both can produce types 1-2 OM particles and all contain a certain amount of Si beside C and O (Li et al., 2012;Posfai et al., 2004;Hand et al., 2005;Adachi and Buseck, 2011). Li et al. (2012) found that primary

Atmos. Chem. Phys. Discuss., doi:10.5194/acp-2016-494, 2016
Manuscript under review for journal Atmos. Chem. Phys.
Published: 23 June 2016

OM particles contain much higher Si from coal combustion than biomass burning. To evaluate OM sources in this study, we compared ratios of Si, O, and C in individual OM particles collected in haze and fresh OM particles from corn stalks and coal combustion conducted in the laboratory (supplementary materials). Figure 8 clearly shows that the Si ratio in individual OM particles is ordered as coal combustion > haze particles > corn stalks; and that 71% of haze OM particles are associated with coal combustion. Therefore, we can conclude that coal combustion contributes more type 1-3 OM particles than biomass burning in the wintertime L&M haze. This result is consistent with the source apportionment of OM particles based on their mass concentrations (Elser et al., 2016;Sun et al., 2013). Furthermore, the consistent Sph and AR of abundant type 1-3 OM particles at the three sampling sites (Table 1) suggests that coal combustion in residential stoves was a widespread emission source from urban to rural areas in the NCP. The vehicular emissions at S1 had a higher contribution of fine soot (i.e., BC) particles with diameters < 300 nm (Fig. 6). Fly ash/metal particles were normally considered from coal-fired power plant and heavy industries (Li and Shao, 2009;Shi et al., 2003;S. X. Wang, 2010). Although fly ash/metal-bearing particles occurred at three sampling sites but their fraction was only 19% (Fig. S7), suggesting that these large stationary sources were not major sources for the primary particles.

4.2 Ageing of OM particles

The complicated mixing structures of individual particles can be used to evaluate particle ageing mechanisms (Li et al., 2016b). Figure 1 suggests that S2 and S3 as the polluted background sites received aged particles after long-range transport and that the urban site of S1 received more fresh particles. Indeed, OM-soot particles at S2 and S3 sites were internally mixed with sulfates but not at S1 (Fig. S8). To evaluate particle ageing processes, we measured OM coating thickness in type 6 OM-coating particles (e.g., Fig. 5e) because coating thickness on secondary particles can be used to infer particle ageing during transport (Moffet et al., 2010;Moffet et al., 2013). In this study, OM coating thickness increased with particle size and that their average

Atmos. Chem. Phys. Discuss., doi:10.5194/acp-2016-494, 2016
Manuscript under review for journal Atmos. Chem. Phys.
Published: 23 June 2016

values at the three sampling sites were ordered as S3 > S2 > S1 (Fig. 9). The results suggest that coarse secondary particles underwent more ageing than the fine particles and that the particles at S3 underwent the most ageing. However, number fractions of type 6 OM particles were small at three sampling sites (14.8% at S2 and 12% at S3, and 2.9% at S1) (Fig. 9). The result indicates weak atmospheric reactions for SOA formation in the whole haze layer.

5. Conclusions and atmospheric implications

Abundant type 1-3 OM particles at S1, S2, and S3 suggested that coal combustion and biomass burning used for cooking and heating in residential sector in winter significantly contributed to the haze layer over the NCP. Although heavy industrial and coal-fired plants emitted large amount of gases such as SO_2, NO_x, and VOCs in the NCP (Wang et al., 2012;Zhang et al., 2015;Wang et al., 2013a), we didn't observe many secondary organic and inorganic aerosols in wintertime L&M hazes; these aerosols are common particle types in heavy haze and fog episodes (Li et al., 2011c). The results indicated very weak photochemical reactions due to lower O_3 concentrations and weaker solar radiation, two constraints that reduce the conversion of the acidic gases into aerosol particles (Ma et al., 2012). Also, the L&M hazes were dry with RH < 60% (Fig. S4), which prohibits heterogeneous reactions between aerosol and gases (Zheng et al., 2015). These reasons can explain why we found higher number and mass fractions of abundant type 1-3 primary OM particles and lower type 6 secondary OM particles in the hazes. This result is consistent with a previous study using AMS (Sun et al., 2013), which showed 69% primary OM particles and only 31% SOA in winter hazes. Concerning mixing processes, the sizes (Fig. 7) and shapes (Sph and AR in Table 1) of the type 1-3 OM particles were consistent with fresh particles at S1 and aged particles at S2 and S3. Therefore, coagulation between OM and non-OM particles was expected to be the major mixing mechanism on the dry haze with its weak photochemistry.

Once humidity exceeds 60% during a haze episode, secondary inorganic and organic species from heterogeneous reactions can significantly contribute to haze

Atmos. Chem. Phys. Discuss., doi:10.5194/acp-2016-494, 2016
Manuscript under review for journal Atmos. Chem. Phys.
Published: 23 June 2016

aerosols (Zheng et al., 2015). In a word, primary emissions from cooking and heating likely caused the regional L&M haze episodes in the NCP. Moreover, coal combustion and biomass burning can emit K-rich sulfates (e.g., Fig. 5d) (Wang et al., 2013b). These residential coal stoves in rural areas and in the urban outskirts have no pollution controls and directly emit particulate carbon and other pollutants. The emission control of residential coarse coal combustion is simply not regulated by the national environmental protection bureau, even though this bureau has made much recent progress in controlling emissions from heavy industries and coal-fired power plants.

We also noticed that a large proportion of type 1-3 primary OM particles has been determined to be brown carbon (BrC), which can absorb shorter-wavelength solar radiation (Alexander et al., 2008). The BrC and BC in the haze layers over the NCP undoubtedly absorb solar energy and influence the vertical mixing of air. One modeling study shows that these absorbing aerosols can lead to a more stable atmospheric stratification over the NCP that decreases turbulence diffusion by 52% and decreases the planetary boundary layer (PBL) height by 33 % (Wang et al., 2015). OM particles from the direct emissions of coarse coal combustion and biomass burning not only contributed to $PM_{2.5}$ in the L&M hazes, but also influenced haze stability. Moreover, the type 1-3 OM particles from coal combustion in residential stoves mainly consist of PAHs (Zhang et al., 2008). In this study, we found that type 1-3 OM particles not only occurred in 70% aerosol particles but also were concentrated on fine particles (< 1 μm) (Fig. 7a). Therefore, these OM-containing particles in the frequent L&M hazes could pose a threat to human health for one long period throughout the winter. Although haze episodes commonly occur in the NCP, the morphology and mixing state of OM particles in the wintertime L&M hazes are largely different from those in the more severe wintertime hazes and from those in L&M hazes in other seasons (Li and Shao, 2009;Li and Shao, 2010). Therefore, these microscopic observations provide important information on the different haze formations and evaluate their atmospheric impacts on climate and human health.

Atmos. Chem. Phys. Discuss., doi:10.5194/acp-2016-494, 2016
Manuscript under review for journal Atmos. Chem. Phys.
Published: 23 June 2016

Acknowledgments

We appreciate Peter Hyde's comments and proofreading. This work was funded by the This research was supported by National Key Project of MOST (JFYS2016ZY01002213), National Natural Science Foundation of China (41575116), Projects of International Cooperation and Exchanges, National Natural Science Foundation of China (41571130033), Shandong Provincial Science Fund for Distinguished Young Scholars, China (JQ201413), and Programs of Shandong University (2014QY001/2015WLJH37).

References

Adachi, K., and Buseck, P. R.: Atmospheric tar balls from biomass burning in Mexico, J. Geophys. Res., 116, 7, doi:10.1029/2010jd015102, 2011.

Adachi, K., Zaizen, Y., Kajino, M., and Igarashi, Y.: Mixing state of regionally transported soot particles and the coating effect on their size and shape at a mountain site in Japan, J. Geophys. Res.-Atmos., 119, 2013JD020880, doi:10.1002/2013jd020880, 2014.

Alexander, D. T. L., Crozier, P. A., and Anderson, J. R.: Brown Carbon Spheres in East Asian Outflow and Their Optical Properties, Science, 321, 833-836, doi:10.1126/science.1155296, 2008.

Chakrabarty, R. K., Moosmüller, H., Chen, L. W. A., Lewis, K., Arnott, W. P., Mazzoleni, C., Dubey, M. K., Wold, C. E., Hao, W. M., and Kreidenweis, S. M.: Brown carbon in tar balls from smoldering biomass combustion, Atmos. Chem. Phys., 10, 6363-6370, doi:10.5194/acp-10-6363-2010, 2010.

Chakrabarty, R. K., Arnold, I. J., Francisco, D. M., Hatchett, B., Hosseinpour, F., Loria, M., Pokharel, A., and Woody, B. M.: Black and brown carbon fractal aggregates from combustion of two fuels widely used in Asian rituals, J. Quant. Spectrosc. Ra., 122, 25-30, doi:10.1016/j.jqsrt.2012.12.011, 2013.

Chen, J., Qiu, S., Shang, J., Wilfrid, O. M., Liu, X., Tian, H., and Boman, J.: Impact of relative humidity and water soluble constituents of PM2. 5 on visibility impairment in Beijing, China, Aerosol Air Qual. Res., 14, 260-268, doi:10.4209/aaqr.2012.12.0360, 2014.

Chi, J. W., Li, W. J., Zhang, D. Z., Zhang, J. C., Lin, Y. T., Shen, X. J., Sun, J. Y., Chen, J. M., Zhang, X. Y., Zhang, Y. M., and Wang, W. X.: Sea salt aerosols as a reactive surface for inorganic and organic acidic gases in the Arctic troposphere, Atmos. Chem. Phys., 15, 11341-11353, doi:10.5194/acp-15-11341-2015, 2015.

China, S., Mazzoleni, C., Gorkowski, K., Aiken, A. C., and Dubey, M. K.: Morphology and mixing state of individual freshly emitted wildfire carbonaceous particles, Nat. Commun, 4, 2122, doi:10.1038/ncomms3122, 2013.

Elser, M., Huang, R. J., Wolf, R., Slowik, J. G., Wang, Q., Canonaco, F., Li, G., Bozzetti, C., Daellenbach, K. R., Huang, Y., Zhang, R., Li, Z., Cao, J., Baltensperger, U., El-Haddad, I., and Prévôt, A. S. H.: New insights into PM2.5 chemical composition and sources in two major cities in China during extreme haze events using aerosol mass spectrometry, Atmos. Chem. Phys., 16, 3207-3225, doi:10.5194/acp-16-3207-2016, 2016.

Fu, P. Q., Kawamura, K., Chen, J., Li, J., Sun, Y. L., Liu, Y., Tachibana, E., Aggarwal, S. G., Okuzawa, K., Tanimoto, H., Kanaya, Y., and Wang, Z. F.: Diurnal variations of organic molecular tracers and stable carbon isotopic composition in atmospheric aerosols over Mt. Tai in the North China Plain: an influence of biomass burning, Atmos. Chem. Phys., 12, 8359-8375, doi:10.5194/acp-12-8359-2012, 2012.

Fuzzi, S., Andreae, M. O., B. J. Huebert, M. Kulmala, T. C. Bond, M. Boy, S. J. Doherty, A. Guenther, M. Kanakidou, K. Kawamura, V.-M. Kerminen, U. Lohmann, L. M. Russell, and Pöschl, U.: Critical assessment of the current state of scientific knowledge, terminology, and research needs concerning the role of organic aerosols in the atmosphere, climate, and global change, Atmos. Chem. Phys., 6, 2017-2038, 2006.

Ghosal, S., Weber, P. K., and Laskin, A.: Spatially resolved chemical imaging of individual atmospheric particles using nanoscale imaging mass spectrometry: insight into particle origin and chemistry, Anal. Methods, 6, 2444-2451, doi:10.1039/c3ay42012d, 2014.

Guo, S., Hu, M., Zamora, M. L., Peng, J., Shang, D., Zheng, J., Du, Z., Wu, Z., Shao, M., Zeng, L., Molina, M. J., and Zhang, R.: Elucidating severe urban haze formation in China, P. Natl. Acad. Sci. USA, 111, 17373-17378, doi:10.1073/pnas.1419604111, 2014.

Hand, J. L., Malm, W. C., Laskin, A., Day, D., Lee, T., Wang, C., Carrico, C., Carrillo, J., Cowin, J. P., Collett, J., and Iedema, M. J.: Optical, physical, and chemical properties of tar balls observed during the Yosemite Aerosol Characterization Study, J. Geophys. Res., 110, doi:10.1029/2004jd005728, 2005.

Huang, R. J., Zhang, Y., Bozzetti, C., Ho, K. F., Cao, J. J., Han, Y., Daellenbach, K. R., Slowik, J. G., Platt, S. M., Canonaco, F., Zotter, P., Wolf, R., Pieber, S. M., Bruns, E. A., Crippa, M., Ciarelli, G., Piazzalunga, A., Schwikowski, M., Abbaszade, G., Schnelle-Kreis, J., Zimmermann, R., An, Z., Szidat, S., Baltensperger, U., El Haddad, I., and Prevot, A. S.: High secondary aerosol contribution to particulate pollution during haze events in China, Nature, 514, 218-222, doi:10.1038/nature13774, 2014.

Kanakidou, M., Seinfeld, J. H., Pandis, S. N., Barnes, I., Dentener, F. J., Facchini, M. C., Van Dingenen, R., Ervens, B., Nenes, A., Nielsen, C. J., Swietlicki, E., Putaud, J. P., Balkanski, Y., Fuzzi, S., Horth, J., Moortgat, G. K., Winterhalter, R., Myhre, C. E. L., Tsigaridis, K., Vignati, E., Stephanou, E. G., and Wilson, J.: Organic aerosol and global climate modelling: a review, Atmos. Chem. Phys., 5, 1053-1123, doi:10.5194/acp-5-1053-2005, 2005.

Kulmala, M., Kerminen, V.-M., Anttila, T., Laaksonen, A., and O'Dowd, C. D.: Organic aerosol formation via sulphate cluster activation, J. Geophys. Res.-Atmos., 109, D04205, doi:10.1029/2003JD003961, 2004.

Li, K., Sinha, B., and Hoppe, P.: Speciation of Nitrogen-Bearing Species Using Negative and Positive Secondary Ion Spectra with Nano Secondary Ion Mass Spectrometry, Anal. Chem., 88, 3281–3288, doi:10.1021/acs.analchem.5b04740, 2016a.

Li, W., Li, P., Sun, G., Zhou, S., Yuan, Q., and Wang, W.: Cloud residues and interstitial aerosols from non-precipitating clouds over an industrial and urban area in northern China, Atmos. Environ., 45, 2488-2495, doi:10.1016/j.atmosenv.2011.02.044, 2011a.

Li, W., Shi, Z., Zhang, D., Zhang, X., Li, P., Feng, Q., Yuan, Q., and Wang, W.: Haze particles over a coal-burning region in the China Loess Plateau in winter: Three flight missions in December 2010, J. Geophys. Res., 117, D12306, doi:10.1029/2012jd017720, 2012.

Li, W., Wang, T., Zhou, S., Lee, S., Huang, Y., Gao, Y., and Wang, W.: Microscopic Observation of Metal-Containing Particles from Chinese Continental Outflow

Observed from a Non-Industrial Site, Environ. Sci. Technol., 47, 9124-9131, doi:10.1021/es400109q, 2013.

Li, W., Shao, L., Zhang, D., Ro, C.-U., Hu, M., Bi, X., Geng, H., Matsuki, A., Niu, H., and Chen, J.: A review of single aerosol particle studies in the atmosphere of East Asia: morphology, mixing state, source, and heterogeneous reactions, J. Clean. Prod., 112, 1330-1349, doi:10.1016/j.jclepro.2015.04.050, 2016b.

Li, W. J., and Shao, L. Y.: Transmission electron microscopy study of aerosol particles from the brown hazes in northern China, J. Geophys. Res., 114, doi:10.1029/2008JD011285, doi:10.1029/2008JD011285, 2009.

Li, W. J., and Shao, L. Y.: Mixing and water-soluble characteristics of particulate organic compounds in individual urban aerosol particles, J. Geophys. Res., 115, doi:10.1029/2009JD012575, 2010.

Li, W. J., Zhang, D. Z., Shao, L. Y., Zhou, S. Z., and Wang, W. X.: Individual particle analysis of aerosols collected under haze and non-haze conditions at a high-elevation mountain site in the North China plain, Atmos. Chem. Phys., 11, 11733-11744, doi:10.5194/acp-11-11733-2011, 2011b.

Li, W. J., Zhou, S. Z., Wang, X. F., Xu, Z., Yuan, C., Yu, Y. C., Zhang, Q. Z., and Wang, W. X.: Integrated evaluation of aerosols from regional brown hazes over northern China in winter: Concentrations, sources, transformation, and mixing states, J. Geophys. Res., 116, doi:10.1029/2010JD015099, doi:10.1029/2010jd015099, 2011c.

Ma, J., Xu, X., Zhao, C., and Yan, P.: A review of atmospheric chemistry research in China: Photochemical smog, haze pollution, and gas-aerosol interactions, Advances in Atmos. Sci., 29, 1006-1026, doi:10.1007/s00376-012-1188-7, 2012.

Mauderly, J. L., and Chow, J. C.: Health Effects of Organic Aerosols, Inhal. Toxicol., 20, 257-288, doi:10.1080/08958370701866008, 2008.

Moffet, R. C., Henn, T. R., Tivanski, A. V., Hopkins, R. J., Desyaterik, Y., Kilcoyne, A. L. D., Tyliszczak, T., Fast, J., Barnard, J., Shutthanandan, V., Cliff, S. S., Perry, K. D., Laskin, A., and Gilles, M. K.: Microscopic characterization of carbonaceous aerosol

particle aging in the outflow from Mexico City, Atmos. Chem. Phys., 10, 961-976, doi:10.5194/acp-10-961-2010, 2010.

Moffet, R. C., Rödel, T. C., Kelly, S. T., Yu, X. Y., Carroll, G. T., Fast, J., Zaveri, R. A., Laskin, A., and Gilles, M. K.: Spectro-microscopic measurements of carbonaceous aerosol aging in Central California, Atmos. Chem. Phys., 13, 10445-10459, doi:10.5194/acp-13-10445-2013, 2013.

Poschl, U.: Atmospheric aerosols: composition, transformation, climate and health effects, Angew Chem Int Ed Engl, 44, 7520-7540, doi:10.1002/anie.200501122, 2005.

Posfai, M., Gelencser, A., Simonics, R., Arato, K., Li, J., Hobbs, P. V., and Buseck, P. R.: Atmospheric tar balls: Particles from biomass and biofuel burning, J. Geophys. Res.-Atmos., 109, doi:10.1029/2003JD004169., doi:10.1029/2003JD004169, 2004.

Riipinen, I., Pierce, J. R., Yli-Juuti, T., Nieminen, T., Hakkinen, S., Ehn, M., Junninen, H., Lehtipalo, K., Petaja, T., Slowik, J., Chang, R., Shantz, N. C., Abbatt, J., Leaitch, W. R., Kerminen, V. M., Worsnop, D. R., Pandis, S. N., Donahue, N. M., and Kulmala, M.: Organic condensation: a vital link connecting aerosol formation to cloud condensation nuclei (CCN) concentrations, Atmos. Chem. Phys., 11, 3865-3878, doi:10.5194/acp-11-3865-2011, 2011.

S. X. Wang, L. Z., G. H. Li, Y. Wu, J. M. Hao, N. Pirrone, F. Sprovieri, and M. P. Ancora: Mercury emission and speciation of coal-fired power plants in China, Atmos. Chem. Phys., 10, 1183–1192, doi:10.5194/acp-10-1183-2010, 2010.

Shen, X. J., Sun, J. Y., Zhang, X. Y., Zhang, Y. M., Zhang, L., Che, H. C., Ma, Q. L., Yu, X. M., Yue, Y., and Zhang, Y. W.: Characterization of submicron aerosols and effect on visibility during a severe haze-fog episode in Yangtze River Delta, China, Atmos. Environ., 120, 307-316, doi:10.1016/j.atmosenv.2015.09.011, 2015.

Shi, Z., Shao, L., Jones, T. P., Whittaker, A. G., Lu, S., Berube, K. A., He, T., and Richards, R. J.: Characterization of airborne individual particles collected in an urban area, a satellite city and a clean air area in Beijing, 2001, Atmos. Environ., 37, 4097-4108, doi:10.1016/S1352-2310(03)00531-4, 2003.

Shiraiwa, M., Ammann, M., Koop, T., and Pöschl, U.: Gas uptake and chemical aging of semisolid organic aerosol particles, P. Natl. Acad. Sci. USA, 108, 11003-11008, doi: 10.1073/pnas.1103045108, 2011.

Sun, Y. L., Zhang, Q., Anastasio, C., and Sun, J.: Insights into secondary organic aerosol formed via aqueous-phase reactions of phenolic compounds based on high resolution mass spectrometry, Atmos. Chem. Phys., 10, 4809-4822, doi:10.5194/acp-10-4809-2010, 2010.

Sun, Y. L., Wang, Z. F., Fu, P. Q., Yang, T., Jiang, Q., Dong, H. B., Li, J., and Jia, J. J.: Aerosol composition, sources and processes during wintertime in Beijing, China, Atmos. Chem. Phys., 13, 4577-4592, doi:10.5194/acp-13-4577-2013, 2013.

Tie, X., Zhang, Q., He, H., Cao, J., Han, S., Gao, Y., Li, X., and Jia, X. C.: A budget analysis of the formation of haze in Beijing, Atmos. Environ., 100, 25-36, doi:10.1016/j.atmosenv.2014.10.038, 2015.

Wang, G., Kawamura, K., Xie, M., Hu, S., Cao, J., An, Z., Waston, J. G., and Chow, J. C.: Organic Molecular Compositions and Size Distributions of Chinese Summer and Autumn Aerosols from Nanjing: Characteristic Haze Event Caused by Wheat Straw Burning, Environ. Sci. Technol., 43, 6493-6499, doi:10.1021/es803086g, 2009.

Wang, H., Shi, G. Y., Zhang, X. Y., Gong, S. L., Tan, S. C., Chen, B., Che, H. Z., and Li, T.: Mesoscale modelling study of the interactions between aerosols and PBL meteorology during a haze episode in China Jing–Jin–Ji and its near surrounding region – Part 2: Aerosols' radiative feedback effects, Atmos. Chem. Phys., 15, 3277-3287, doi:10.5194/acp-15-3277-2015, 2015.

Wang, J., Zhang, Y., Shao, M., Liu, X., Zheng, L., Cheng, C., and Xu, X.: Quantitative relationship between visibility and mass concentration of PM2. 5 in Beijing, J. Environ. Sci., 18, 475-481, 2006.

Wang, M., Shao, M., Lu, S.-H., Yang, Y.-D., and Chen, W.-T.: Evidence of coal combustion contribution to ambient VOCs during winter in Beijing, Chinese Chem. Lett., 24, 829-832, doi:10.1016/j.cclet.2013.05.029, 2013a.

Wang, X., Wang, W., Yang, L., Gao, X., Nie, W., Yu, Y., Xu, P., Zhou, Y., and Wang, Z.: The secondary formation of inorganic aerosols in the droplet mode through heterogeneous aqueous reactions under haze conditions, Atmos. Environ., 63, 68-76, doi:10.1016/j.atmosenv.2012.09.029, 2012.

Wang, X., Williams, B. J., Tang, Y., Huang, Y., Kong, L., Yang, X., and Biswas, P.: Characterization of organic aerosol produced during pulverized coal combustion in a drop tube furnace, Atmos. Chem. Phys., 13, 10919-10932, doi:10.5194/acp-13-10919-2013, 2013b.

You, Y., Renbaum-Wolff, L., Carreras-Sospedra, M., Hanna, S. J., Hiranuma, N., Kamal, S., Smith, M. L., Zhang, X., Weber, R. J., Shilling, J. E., Dabdub, D., Martin, S. T., and Bertram, A. K.: Images reveal that atmospheric particles can undergo liquid–liquid phase separations, P. Natl. Acad. Sci. USA, 109, 13188-13193, doi: 10.1073/pnas.1206414109, 2012.

Yuan, Q., Li, W., Zhou, S., Yang, L., Chi, J., Sui, X., and Wang, W.: Integrated evaluation of aerosols during haze-fog episodes at one regional background site in North China Plain, Atmos. Res., 156, 102-110, doi:10.1016/j.atmosres.2015.01.002, 2015.

Zawadowicz, M. A., Proud, S. R., Seppalainen, S. S., and Cziczo, D. J.: Hygroscopic and phase separation properties of ammonium sulfate/organics/water ternary solutions, Atmos. Chem. Phys., 15, 8975-8986, doi:10.5194/acp-15-8975-2015, 2015.

Zhang, Q., Jimenez, J. L., Canagaratna, M. R., Allan, J. D., Coe, H., Ulbrich, I., Alfarra, M. R., Takami, A., Middlebrook, A. M., Sun, Y. L., Dzepina, K., Dunlea, E., Docherty, K., DeCarlo, P. F., Salcedo, D., Onasch, T., Jayne, J. T., Miyoshi, T., Shimono, A., Hatakeyama, S., Takegawa, N., Kondo, Y., Schneider, J., Drewnick, F., Borrmann, S., Weimer, S., Demerjian, K., Williams, P., Bower, K., Bahreini, R., Cottrell, L., Griffin, R. J., Rautiainen, J., Sun, J. Y., Zhang, Y. M., and Worsnop, D. R.: Ubiquity and dominance of oxygenated species in organic aerosols in anthropogenically-influenced Northern Hemisphere midlatitudes, Geophys. Res. Lett., 34, L13801, doi:10.1029/2007gl029979, 2007.

Zhang, X. Y., Wang, J. Z., Wang, Y. Q., Liu, H. L., Sun, J. Y., and Zhang, Y. M.: Changes in chemical components of aerosol particles in different haze regions in China from 2006 to 2013 and contribution of meteorological factors, Atmos. Chem. Phys., 15, 12935-12952, doi:10.5194/acp-15-12935-2015, 2015.

Zhang, Y., Schauer, J. J., Zhang, Y., Zeng, L., Wei, Y., Liu, Y., and Shao, M.: Characteristics of particulate carbon emissions from real-world Chinese coal combustion, Environ. Sci. Technol., 42, 5068-5073, doi:10.1021/es7022576, 2008.

Zheng, G. J., Duan, F. K., Su, H., Ma, Y. L., Cheng, Y., Zheng, B., Zhang, Q., Huang, T., Kimoto, T., Chang, D., Poschl, U., Cheng, Y. F., and He, K. B.: Exploring the severe winter haze in Beijing: the impact of synoptic weather, regional transport and heterogeneous reactions, Atmos. Chem. Phys., 15, 2969-2983, doi:10.5194/acp-15-2969-2015, 2015.

Zhu, J., Crozier, P. A., and Anderson, J. R.: Characterization of light-absorbing carbon particles at three altitudes in East Asian outflow by transmission electron microscopy, Atmos. Chem. Phys., 13, 6359-6371, doi:10.5194/acp-13-6359-2013, 2013.

Atmos. Chem. Phys. Discuss., doi:10.5194/acp-2016-494, 2016
Manuscript under review for journal Atmos. Chem. Phys.
Published: 23 June 2016

Figure Captions

Figure 1. Cluster-means of backward trajectories at S1 (urban Jinan), S2 (Mt. Tai top), and S3 (Changdao island) sites during 13-23 December, 2014. Air masses on clear days normally are from the northwest and air masses on haze days are from the west or southwest. MODIS images show the layer during the light and moderate regional hazes over the NCP.

Figure 2. NanoSIMS-based ion intensity mappings of $^{12}C^{14}N^-$, $^{14}N^{16}O_2^-$, $^{16}O^-$, and $^{32}S^-$ from a near-spherical OM particle.

Figure 3. Typical TEM images of different types of OM particles. (a) Type 1: spherical shape; (b) type 2: near-spherical shape; (c) type 3: irregular shape; (d) type 4: domelike OM (droplet-like particle); (e) type 5: dispersed-OM; (f) type 6: OM-coating

Figure 4. Number fraction of OM types in particulate matter during light and moderate haze episodes from 13 to 23 December 2014. The 2562 OM particles were analyzed by TEM-EDX.

Figure 5. Typical TEM images of OM internally mixed particles (a) a spherical OM particle attached to a soot particle; (b) a near-spherical OM particle attached to a mineral particle; (c) fly ash particles attached to a near-spherical OM particle; (d) OM mixed with sulfate (K)-fly ash particle and its sublimed particle under strong electron beam; (e) OM as a coating mixed with a sulfate (K, Na) particle. The element compositions in OM, mineral, fly ash, and sulfate particles were measured by the TEM/EDX.

Figure 6. Number fraction of OM internally mixed particles at (a) S1 site, (b) S2 site, and (c) S3 site. The number of analyzed particles in different size ranges is shown above each column.

Figure 7. Size distributions of OM-containing particles and OM particles during the same hazes. (a) Size distributions of 1088, 1341 and 1136 OM-containing particles collected at S1, S2, and S3. (b) Size distributions of 269, 173, and 297 type 1-3 OM particles collected at S1, S2, and S3.

Atmos. Chem. Phys. Discuss., doi:10.5194/acp-2016-494, 2016
Manuscript under review for journal Atmos. Chem. Phys.
Published: 23 June 2016

Figure 8. Triangular diagram of weight ratios of Si-O-C based on TEM/EDX data. 34 OM particles from coal combustion and 28 OM particles from corn stalks combustion, and 281 OM particles produced from the haze samples in this study. The three lines represent the links of the ratios of Si/O and Si/C in haze, corn stalks and coal combustion samples, respectively.

Figure 9. The relationship between the size of individual particles and their sulfate cores based on 366 OM-coating particles at S1, S3, and S3 sites. The smaller slope represents the thicker OM coating. The number fractions of OM coating to OM-containing particles at three sampling sites are shown in the pie charts.

Atmos. Chem. Phys. Discuss., doi:10.5194/acp-2016-494, 2016
Manuscript under review for journal Atmos. Chem. Phys.
Published: 23 June 2016

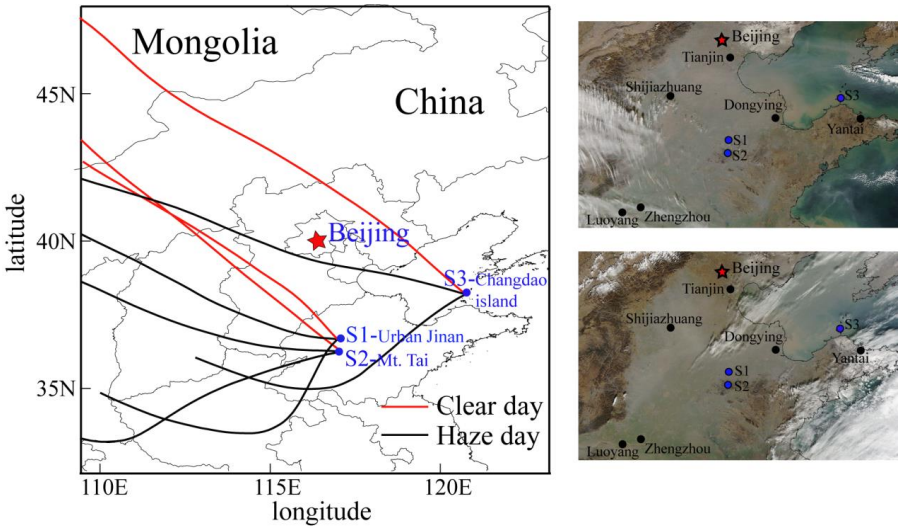

Figure 1. Cluster-means of backward trajectories at S1 (urban Jinan), S2 (Mt. Tai top), and S3 (Changdao island) sites during 13-23 December, 2014. Air masses on clear days normally are from the northwest and air masses on haze days are from the west or southwest. MODIS images show the layer during the light and moderate regional hazes over the NCP.

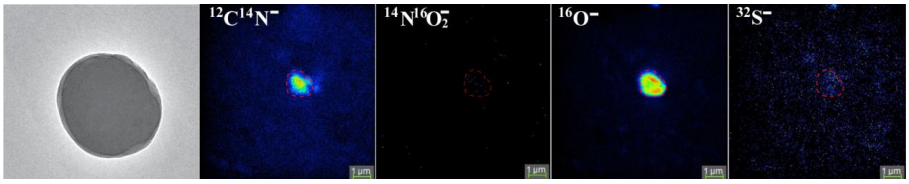

Figure 2. NanoSIMS-based ion intensity mappings of $^{12}C^{14}N^-$, $^{14}N^{16}O_2^-$, $^{16}O^-$, and $^{32}S^-$ from a near-spherical OM particle.

Atmos. Chem. Phys. Discuss., doi:10.5194/acp-2016-494, 2016
Manuscript under review for journal Atmos. Chem. Phys.
Published: 23 June 2016

Atmospheric Chemistry and Physics Discussions
Open Access

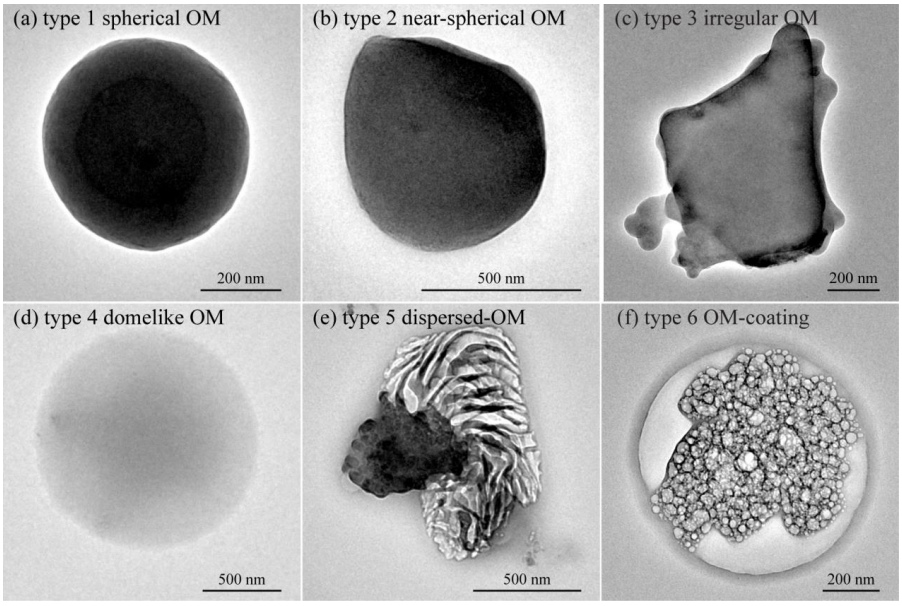

Figure 3. Typical TEM images of different types of OM particles. (a) Type 1: spherical shape; (b) type 2: near-spherical shape; (c) type 3: irregular shape; (d) type 4: domelike OM (droplet-like particle); (e) type 5: dispersed-OM; (f) type 6: OM-coating

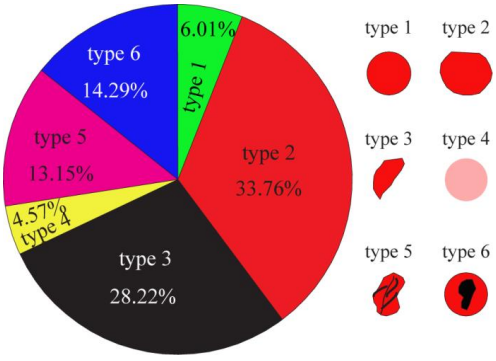

Figure 4. Number fraction of OM types in particulate matter during light and moderate haze episodes from 13 to 23 December 2014. The 2562 OM particles were analyzed by TEM-EDX.

Atmos. Chem. Phys. Discuss., doi:10.5194/acp-2016-494, 2016
Manuscript under review for journal Atmos. Chem. Phys.
Published: 23 June 2016

Atmospheric Chemistry and Physics
Discussions
Open Access

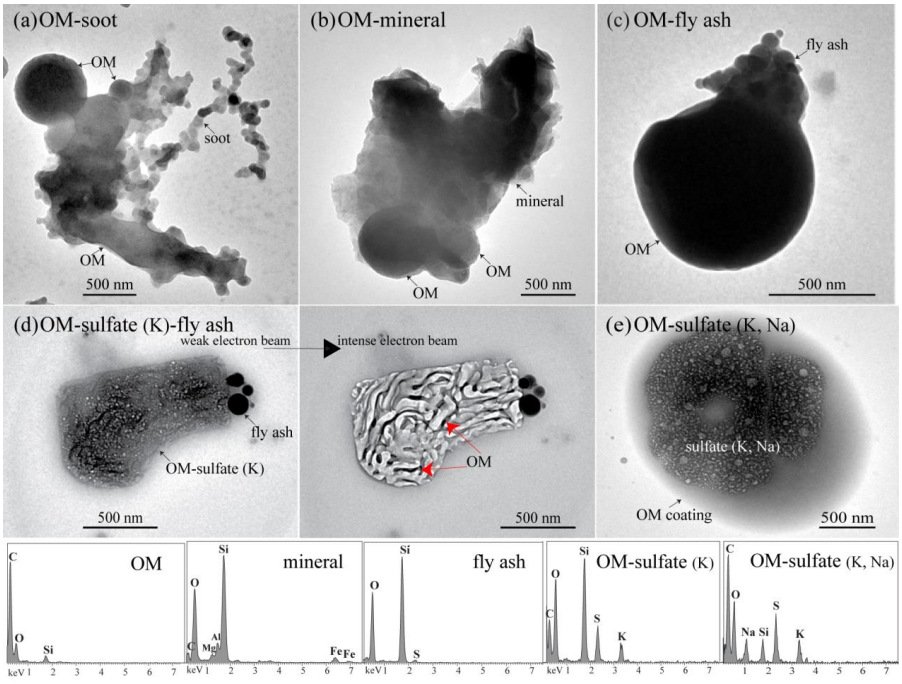

Figure 5. Typical TEM images of OM internally mixed particles (a) a spherical OM particle attached to a soot particle; (b) a near-spherical OM particle attached to a mineral particle; (c) fly ash particles attached to a near-spherical OM particle; (d) OM mixed with sulfate (K)-fly ash particle and its sublimed particle under strong electron beam; (e) OM as a coating mixed with a sulfate (K, Na) particle. The element compositions in OM, mineral, fly ash, and sulfate particles were measured by the TEM/EDX.

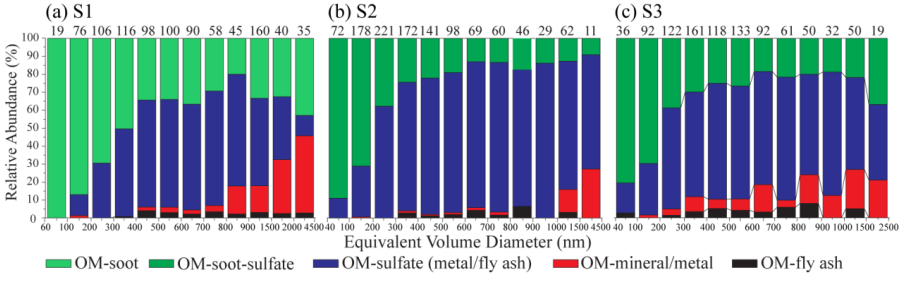

Atmos. Chem. Phys. Discuss., doi:10.5194/acp-2016-494, 2016
Manuscript under review for journal Atmos. Chem. Phys.
Published: 23 June 2016

Figure 6. Number fraction of OM internally mixed particles at (a) S1 site, (b) S2 site, and (c) S3 site. The number of analyzed particles in different size ranges is shown above each column.

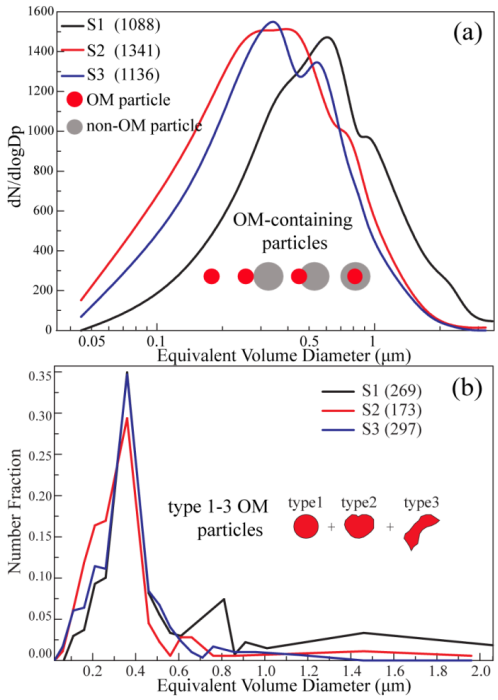

Figure 7. Size distributions of OM-containing particles and OM particles during the same hazes. (a) Size distributions of 1088, 1341 and 1136 OM-containing particles collected at S1, S2, and S3. (b) Size distributions of 269, 173, and 297 type 1-3 OM particles collected at S1, S2, and S3.

Atmos. Chem. Phys. Discuss., doi:10.5194/acp-2016-494, 2016
Manuscript under review for journal Atmos. Chem. Phys.
Published: 23 June 2016

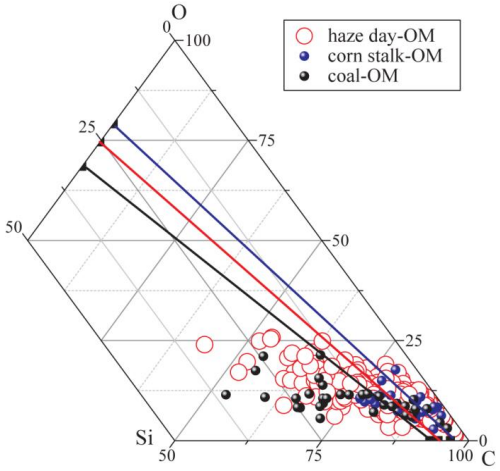

Figure 8. Triangular diagram of weight ratios of Si-O-C based on TEM/EDX data. 34 OM particles from coal combustion and 28 OM particles from corn stalks combustion, and 281 OM particles produced from the haze samples in this study. The three lines represent the links of the ratios of Si/O and Si/C in haze, corn stalks and coal combustion samples, respectively.

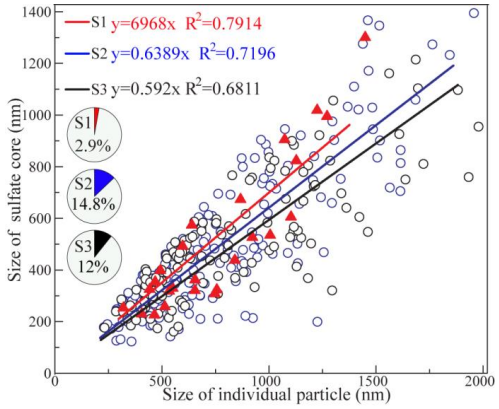

Figure 9. The relationship between the size of individual particles and their sulfate cores based on 366 OM-coating particles at S1, S3, and S3 sites. The smaller slope represents the thicker OM coating. The number fractions of OM coating to OM-containing particles at three sampling sites are shown in the pie charts.

Atmos. Chem. Phys. Discuss., doi:10.5194/acp-2016-494, 2016
Manuscript under review for journal Atmos. Chem. Phys.
Published: 23 June 2016

Atmospheric Chemistry and Physics Discussions

Table 1. Average size, number, sphericity, and aspect ratio for different OM types at the three sampling sites.

Sampling site	Type	Average Size（nm）	Number	Average Sph (min, max); (±stdev.)	Average AR (min, max); (±stdev.)
S1	Type1 spherical	407.8	18	0.9664 (0.8, 1.0); (±0.05)	1.0223 (1.0, 1.16); (±0.03)
	Type2 near spherical	348.5	79	0.8172 (0.50, 1); (±0.11)	1.1275 (1.0, 1.41); (±0.08)
	Type3 irregular	538.68	151	0.5046 (0.07,0.95); (±0.21)	1.4764 (1.04, 3.57); (±0.41)
	Type4 domelike	758.76	23	0.6374 (0.29, 0.9); (±0.21)	1.3958 (1.08, 1.89); (±0.26)
	Type5 dispersed-OM	750.8	64	0.4940 (0.1, 0.92); (±0.21)	1.4646 (1.06, 2.85); (±0.40)
	Type6 OM-coating	672.18	12	0.9251(0.45, 1); (±0.13)	1.0627 (1, 1.45); (±0.11)
S2	Type1 spherical	282.15	22	0.9628 (0.76, 1.0); (±0.06)	1.0281 (1.00, 1.25); (±0.05)
	Type2 near spherical	323.15	68	0.8254 (0.53, 1.0); (±0.12)	1.1197 (1.00, 1.37); (±0.09)
	Type3 irregular	399.26	62	0.5746 ((0.06,0.96); (±0.24)	1.4102 (1.04, 2.79); (±0.42)
	Type4-domelike	511.35	25	0.7341 (0.15, 1.0); (±0.29)	1.2433 (1.00, 2.28); (±0.36)
	Type5-dispersed-OM	846.99	34	0.5773 (0.1, 0.9); (±0.25)	1.4218 (1.08, 2.71) (±0.45)
	Type6-OM-coating	775.53	66	0.8791 (0.26, 1) (±0.22)	1.0797 (1, 1.57) (±0.12)
S3	Type1 spherical	391.5	27	0.9901 (0.92, 1.0); (±0.02)	1.0065 (1.0, 1.06); (±0.02)
	Type2 near spherical	373.09	122	0.8341 (0.33, 1.0); (±0.13)	1.12 (1,1.51); (±0.10)
	Type3 irregular	374.85	117	0.5675 (0.09, 0.96); (±0.21)	1.392 (1.04, 2.82); (±0.34)
	Type4 domelike	705.94	14	0.6325 (0.22, 1); (±0.23)	1.3519 (1, 1.857); (±0.22)
	Type5 dispersed-OM	574.62	35	0.5495 (0.4,0.65); (±0.19)	1.3475 (1.21, 1.51); (±0.31)
	Type6 OM-coating	828.35	28	0.9291 (0.36,1); (±0.30)	1.0591 (1.0, 1.60); (±0.14)